Article

Not peer-reviewed version

3D Bioprinting of Alginate-Based Hydrogels to Investigate Osteogenic Differentiation of hBMSCS *In Vitro*

Ana Catarina Sousa , Grace Mcdermott , Fraser Shields , Rui Alvites , Bruna Lopes , Patrícia Sousa , Alícia Moreira , André Coelho , José Domingos Santos , Luís Atayde , Nuno Alves , Stephen Richardson , Marco A.N Domingos , Ana Colette Maurício *

Posted Date: 12 August 2024

doi: 10.20944/preprints202408.0693.v1

Keywords: alginate; BioInk; bioprinting; bone regeneration; collagen; hydroxyapatite; human bone marrow stem/stromal cells

 doi:10.20944/preprints202408.0693.v1

Article

3D Bioprinting of Alginate-Based Hydrogels to Investigate Osteogenic Differentiation of hBMSCS *In Vitro*

Ana Catarina Sousa [1,2,3], Grace Mcdermott [4], Fraser Shields [4], Rui Alvites [1,2,3,5], Bruna Lopes [1,2,3], Patrícia Sousa [1,2,3], Alícia Moreira [1,2,3], André Coelho [1,2,3], José Domingos Santos [6], Luís Atayde [1,2,3], Nuno Alves [7], Stephen Richardson [4], Marco A.N Domingos [8] and Ana Colette Maurício [1,2,3]*

[1] Departamento de Clínicas Veterinárias, Instituto de Ciências Biomédicas de Abel Salazar (ICBAS), Universidade do Porto (UP), Rua de Jorge Viterbo Ferreira, nº 228, 4050-313 Porto, Portugal
[2] Centro de Estudos de Ciência Animal (CECA), Instituto de Ciências, Tecnologias e Agroambiente da Universidade do Porto (ICETA), Rua D. Manuel II, Apartado 55142, 4051-401, Porto, Portugal
[3] Associate Laboratory for Animal and Veterinary Science (AL4AnimalS), Lisboa, Portugal.
[4] Department of Cell Matrix Biology & Regenerative Medicine, Faculty of Biology, Medicine & Health, The University of Manchester, Manchester M13 9PL, UK
[5] Instituto Universitário de Ciências da Saúde (CESPU), Avenida Central de Gandra 1317, Gandra, 4585-116 Paredes, Portugal.
[6] REQUIMTE-LAQV, Departamento de Engenharia Metalúrgica e Materiais, Faculdade de Engenharia, UP
[7] Centre for Rapid and Sustainable Product Development (CDRSP), Polytechnic Institute of Leiria, Portugal
[8] Department of Mechanical and Aerospace Engineering, School of Engineering, Faculty of Science and Engineering & Henry Royce Institute, The University of Manchester, Manchester M13 9PL, UK
* Correspondence: ana.colette@hotmail.com or acmauricio@icbas.up.pt (A.C.M.)

Abstract: Three-dimensional (3D) models with improved biomimicry are essential to reduce animal experimentation and drive innovation in tissue engineering. In the current study, we investigate the use of alginate-based materials as polymeric inks for 3D bioprinting of osteogenic models using human bone marrow stem/stromal cells (hBMSCs). A composite bioink incorporating alginate, nano-hydroxyapatite (nHA), type I collagen (Col) and hBMSCs was developed and for extrusion-based printing. Rheological tests perfomed on crosslinked hydrogels confirm the formation of solid-like structures consistently indicating a higher storage modulus compared to the loss modulus. The swelling behaviour analysis showed that the addition of Col and nHA into an alginate matrix can enhance the swelling rate of the resulting composite hydrogels, which maximizes cell proliferation within the structure. The LIVE/DEAD assay outcomes demonstrate that the inclusion of nHA and Col did not detrimentally affect the viability of hBMSCs over seven days post-printing. PrestoBlueTM revealed a higher hBMSCs viability in the alginate-nHA-Col hydrogel compared to the remaining groups. Gene expression analysis revealed that alginate-nHA-col bioink favoured a higher expression of osteogenic markers, including secreted phosphoprotein-1 (SPP1) and collagen type 1 alpha 2 chain (COL1A2), in hBMSCs after 14 days, indicating the pro-osteogenic differentiation potential of the hydrogel. This study demonstrates that the incorporation of nHA and Col into alginate enhances osteogenic potential and provides a bioprinted model to systematically study osteogenesis and the early stages of tissue maturation *in vitro*.

Keywords: alginate; BioInk; bioprinting; bone regeneration; collagen; hydroxyapatite; human bone marrow stem/stromal cells

1. Introduction

Bone diseases are an important global public health problem that have significant economic effects, particularly for people suffering from osteoporosis [1–3]. Research models that replicate the bone structure, its functions, the cell-cell and cell-matrix interactions that occur *in vivo* have been developed to ensure the clinical translation of new treatments to more reliably treat these bone

 doi:10.20944/preprints202408.0693.v1

pathologies [4]. Considering the challenge of bone's complexity, in the last decade there has been growing interest in developing 3D models that mimic the bone microenvironment aiming to reduce or replace the dependence on animal experiments [5].

The field of bioprinting has emerged as a transformative approach within regenerative medicine and tissue engineering, demonstrating significant potential for the generation of three-dimensional tissue constructs [6]. A noteworthy application of this technology is in the field of bone tissue regeneration, which has been increasingly emphasized. This is mainly due to the structural and biological complexities that define the nature of bone tissue [7].

Alginate, an FDA-approved natural polysaccharide, is widely employed in biomedical applications as a bioink [8,9]. This widespread use is attributed to its low cost [10], accessibility [11], and ease of preparation [12]. Consequently, alginate-based hydrogels emerge as a promising candidate capable of offering a three-dimensional (3D) microenvironment encompassing both organic and inorganic elements vital for osteoblast functionality. Nevertheless, alginate is an inert material and lacks osteoinductive signals necessary for promoting osteoblast differentiation and bone formation. To address these limitations, additional modifications are required to enhance its osteogenic potential. Combining alginate with collagen (Col), the primary structural component of the extracellular matrix (ECM), and bioactive ceramics, such as hydroxyapatite (HA), can significantly increase osteoconductivity [10,13,14]. These materials were selected due to bone's hierarchical structure, consisting of living cells immersed in a matrix primarily composed of Col and HA [15]. Researchers focus on mimicking the bone's composition to achieve a high degree of similarity between the 3D printed scaffold and bone tissue. Col represents nearly 80% of the organic material in bones [16,17]. It is a suitable biomaterial due to its outstanding biocompatibility, degradability, adhesion characteristics, osteogenic induction properties, and minimal immunogenicity [18]. Additionally, nano-HA (nHA) presents stability, biocompatibility, hydrophilicity, and degradability. This ceramic enhances the adhesion and proliferation of osteoblasts and possesses the capacity to establish chemical bonds with the surrounding bone tissue [19]. The combination of alginate, a biocompatible polymer capable of forming stable gels, nHA, an osteoconductive element, and Col, a primary organic component of natural bone, has been demonstrated to improve the biomineralization, promoting natural bone regeneration [20]. These biomaterials have been utilized in bone bioprinting applications to replicate the complex hierarchical structure of bone tissue, which is essential for its biological functions [21–24]. Hassani *et al.* developed cell-laden alginate-nHA-Col microcapsules for modular bone tissue and the results suggest that this structure promotes mineralization and the osteogenesis signaling pathways of the encapsulated cells [25].

In the field of regenerative medicine, the integration of biomaterials with mesenchymal stem/stromal cells (MSCs) has been prevalent, as this approach promotes the proliferation and differentiation of MSCs [26,27].These cells can be isolated from several tissues, including bone marrow [28]. Human MSCs derived from bone marrow (hBMSCs) are considered multipotent stromal cells and they possess the inherent capacity to differentiate into osteoblasts and form bone tissue, allowing their osteogenic differentiation to be studied directly in a 3D environment [29,30].

In light of these considerations, the present study aimed to develop a bioink formulation tailored for extrusion-based bioprinting, incorporating alginate, nHA, and Col, along with hBMSCs. This is the first study applying these biomaterials and hBMSCs, through biofabrication (using a pressure-assisted extrusion technique), seeking to address the fundamental challenge of replicating the composition of the native ECM in terms of materials (organic and inorganic) to study osteogenesis in 3D. Therefore, this technique ensures the spatial distribution and cell loading efficiency, facilitates the detailed study of cell-biomaterial interactions, and results in the creation of highly structured and functional tissue constructs. This approach provides a bioprinted model to study osteogenesis and the early stages of tissue maturation *in vitro*. Therefore, the current work highlights the production of a tailored bioink and underlines its significant contribution to the development of a 3D model for studying the osteogenic differentiation of MSCs.

2. Materials and Methods

 doi:10.20944/preprints202408.0693.v1

2.1. Materials

Sodium alginate (#180947-100G), nHA (particle size < 200 nm; #677418-25G) and Col type I (#5074-35ML) were purchased from Sigma-Aldrich (Saint Louis, MO, USA). The hydrogel formulations were prepared using an agarose (#A6013-100G) fluid gel bath also obtained from Sigma-Aldrich (Saint Louis, MO, USA). Subsequent to their production, the hydrogels were cross-linked using calcium chloride dihydrate ($CaCl_2.2H_2O$; #22317.230-250G), from VWR Chemicals (Pennsylvania, USA).

2.2. Preparation of Alginate-Based Solutions

The alginate solution was prepared by dissolving 4% (w/v) sodium alginate in Milli-Q water with continuous magnetic stirring overnight. Following this, the 4% alginate solution underwent sterilization via autoclaving and was subsequently subjected to a 1:1 dilution with Milli-Q water, resulting in the formulation of a 2% alginate solution. For the preparation of the alginate-nHA-Col solution, the 2% (w/v) alginate solution was combined with 0.5% (w/v) nHA and 0.5% (w/v) Col. **Table 1** provides an overview of the compositions of the alginate-based solutions.

Table 1. Composition of alginate-based solutions.

Solutions	Sodium alginate (w/v)	nHA (w/v)	Col (w/v)
Alginate	2	-	-
Alginate-nHA-Col	2	0.5	0.5

2.3. Cell culture and Maintenance

Research manuscripts reporting large datasets that are deposited in a publicly available database should specify where the data have been deposited and provide the relevant accession numbers. If the accession numbers have not yet been obtained at the time of submission, please state that they will be provided during review. They must be provided prior to publication. All experiments followed the relevant guidelines and were conducted with approvals from the NHS Health Research Authority National Research Ethics Service (21/NS/0056) and the University of Manchester, as well as written inform donor consent. The hBMSCs used were isolated from bone marrow obtained from a 49-year-old female donor following hip replacement surgery using a previously published protocol [31]. HBMSCs were maintained under standard conditions, specifically at 37°C in 80% humidified atmosphere containing 5% CO_2. Cells were cultured under standard conditions in αMEM media (Sigma-Aldrich, # M4526) enriched with 10% (v/v) fetal bovine serum (FBS) (Gibco, #A3160802), 110 mg L^{-1} sodium pyruvate, 1000 mg L^{-1} glucose, 100 U mL^{-1} penicillin, 100 µg mL^{-1} streptomycin (Gibco, #15140122) and 0.25 µg mL^{-1} amphotericin (Gibco, #15290026) and 2 mM GlutaMAX (Gibco, #35050061).

2.4. Oscillatory Rheological Measurements

The rheological properties of the hydrogels were determined using an Anton Paar RheoCompass™ rheometer (MCR92, Anton Paar, Graz, Austria) operated with Anton Paar RheoCompass v1.30.1164 software. Measurements were conducted using a PP12.5 measuring plate, featuring a diameter of 12.5 mm and a 1 mm gap. Alginate-based hydrogels with different compositions (as detailed in **Table 1**) were prepared using the transwell methodology. In brief, 400 µL of the solution was pipetted onto 12-well plate transwell inserts. The alginate-nHA-Col hydrogels gelation was induced through a dual-crosslinking procedure. Initially, Col crosslinking was induced by incubating at 37°C for 90 minutes. Subsequently, the alginate was gelled using 150 µM calcium chloride ($CaCl_2$) solution in Milli-Q water for 40 minutes, as the process used for alginate-only hydrogels. Finally, the hydrogels were removed from the inserts and washed with DPBS.

The measurement conditions were as follows: Amplitude Sweep: Temperature =25ºC, Frequency = 1 Hz, Oscillation Strain = 0.01–100%; Frequency Sweep: Temperature =25ºC, Frequency = 0.1 - 10

 doi:10.20944/preprints202408.0693.v1

Hz, Oscillation Strain = 0.1%. The data was measured in triplicate and the results were presented as mean ± standard deviation.

2.5. Hydrogel Swelling Behavior

Hydrogel swelling behavior was assessed under physiological conditions (pH = 7.4 at 37°C). Initially, the weight of the hydrogels (prepared as outlined in section 4.3) was measured post-crosslinking using precision scales (GR-300-EC, A&D Instruments, United Kingdom). Subsequently, these hydrogels were immersed in DPBS at 37°C within a 12-well plate, and the weight of the swollen hydrogels was recorded. At specific time intervals (1, 2, 3, 4, 24, 48, and 72 hours), the hydrogels were reweighed after blotting off excess water with tissue paper. The swelling behavior was quantified as a percentage of the swelling ratio, computed using **Equation I**.

$$\text{Swelling ratio (\%)} = (Wf - Wi)/Wi \times 100, \quad \text{(I)}$$

Wf and Wi are final and initial weight of the hydrogel (in g), respectively.

2.6. Mechanical Analysis

Compressive strength and Young's modulus (expressed in kPa) of the hydrogels were assessed using the ElectroForce 5500® Test instrument (TA Instruments, Delaware, USA) equipped with a 5 N load cell. Alginate and alginate-nHA-Col hydrogels (prepared as outlined in section 2.2 of the Materials and Methods) were tested in triplicate, each sample having a height of 3 mm and a diameter of 12 mm. A compression test was conducted employing a flat probe with a diameter of 10 mm and a cross-head displacement rate of 2.0 mm/min. Compression was continued until 80% strain was reached. The compressive (Young's) modulus was determined by calculating the slope of the linear portion of the stress-strain curve at 10% strain. The settings for the loading procedure were programmed using the WinTest® Software (TA instruments). The real-time monitoring of the applied load was performed using the WinTest® Software.

2.7. Bioprinting of Cell-Laden Hydrogels

A pressure-assisted extrusion printer (3D Discovery, RegenHU, Villaz-St-Pierre, Switzerland) with an enclosed biosafety cabinet was employed in the fabrication of cell-laden constructs (**Figure 1-A**). Alginate-based inks loaded with hBMSCs at a density of 2 x 10^6 cells/mL were prepared as described in the section 2.2 and 2.3 and printed inside a suspension bath of agarose particles (**Figure 1-B**) [32], using a set of process parameters previously optimized in our lab. The suspension bath was prepared based on a protocol originally reported by Moxon *et al.* [33].

Square-based scaffolds (6 x 6 mm) were designed using BioCAM™ software (RegenHU, Villaz-St-Pierre, Switzerland) and printed in 12-well plates under sterile conditions and at room temperature. Post printing, the crosslinking was conducted following a two-step process. First, Col fibrils were allowed to self-assemble for 90 minutes at 37°C. Then, a $CaCl_2$ solution in water was added to the wells and incubated for 40 minutes at 37°C to trigger the crosslinking of the alginate. Cell-laden hydrogels were rinsed with DPBS solution and then cultured in αMEM media at 37°C with 5% CO_2 and 80% humidity.

 doi:10.20944/preprints202408.0693.v1

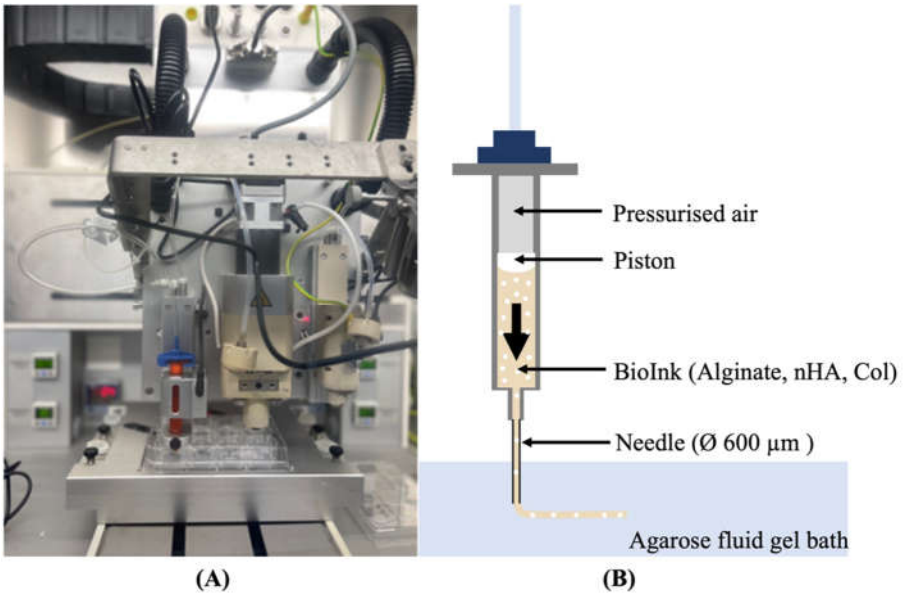

Figure 1. (A) 3D Discovery Evolution bioprinter (RegenHU, Villaz-St-Pierre, Switzerland); (B) Graphical representation of the pressure-assisted extrusion that uses pressurized air to force bioink flow directly from the bioprinter cartridge through a needle into a well plate containing a suspension bath.

2.8. Live/Dead Staining

A Live/Dead assay kit (Invitrogen™ #L3224) was used to evaluate the viability of hBMSCs cultured on alginate and alginate-nHA-Col hydrogels. Following the manufacturer's instructions, 600 µL of the assay solution comprising 4 µM ethidium homodimer^{-1} (EthD^{-1}) and 2 µM calcein AM were dispensed onto the cell-hydrogel constructs. Following 20 minutes of incubation, the cells were washed in DPBS and imaged using a CellVoyager™ CQ1 Benchtop High-Content Analysis System (Yokogawa, Japan) (excitation wavelength: 495 nm). Cell imaging was conducted at one, three, and seven days post-culture, with three images acquired per time point. The acquired images were systematically analysed and subsequently the number of cells quantified using ImageJ2 software (version: 2.3.0/1.53q). Viability was determined by dividing the number of live cells by the total number of cells. All measurements were performed 3 times for each time point to ensure reproducibility.

2.9. Cell Viability Assay

To evaluate the cellular viability of hBMSCs within alginate-based hydrogels, the PrestoBlue™ (InvitrogenTM #A13261) assay was performed at one, three, five, and seven days. The evaluation was performed as previously described [19]. In brief, at each timepoint, the culture media was aspirated and substituted with fresh complete media supplemented with 10% (v/v) of the PrestoBlueTM reagent. After one hour of incubation at 37°C, in a controlled environment with 80% humidity and 5% CO_2, the supernatant media were transferred to a 96-well plate, and absorbance measurements were taken at wavelengths of 570 nm and 595 nm. Alterations in cell viability were quantified using absorbance spectroscopy with a SPARK® multimode microplate reader (TECAN, Männedorf, Switzerland). To calculate the corrected absorbance, the absorbance recorded at 595 nm (as normalization) was subtracted from the absorbance obtained at 570 nm (representing the experimental outcome). Subsequently, the derived values underwent additional adjustment by subtracting the average absorbance measured in control wells from the corresponding experimental wells. The cells were gently washed with DPBS to eliminate any residual substance, and fresh culture medium was then introduced into each well.

2.10. Gene Expression

 doi:10.20944/preprints202408.0693.v1

To quantify gene expression levels, RNA extraction and complementary DNA (cDNA) synthesis were performed following established protocols [29,30]. Quantitative real-time polymerase chain reaction (qPCR) were carried out on a StepOnePlus system (Applied Biosystems), utilizing pre-designed intron-spanning primers (Sigma Aldrich) (**Table 2**). In brief, a total of 10 ng cDNA was added to each reaction in addition to 5µl of Fast SYBR Green Reagent, 1µl of forward primer, 1µl of reverse primer, and 2.5µl of molecular biology grade water.

cDNA synthesized in-house from Total Human RNA (Clontech) served as the positive control in this study. The levels of osteogenic genes were standardized by normalization against the pre-validated reference gene GAPDH [36].

Table 2. Name, accession number, forward/ reverse sequences, and concentrations of the primers used to assess osteogenic differentation.

Primer	Accession Number	Forward Primer Sequence 5′-3′	Reverse Primer Sequence 5′-3′	Concentration (nM)
glyceraldehyde-3-phosphate dehydrogenase (GAPDH)	NM_001256799	CTCCTCTGACTTCAACAG	CGTTGTCATACCAGGAAA	600
runt-related transcription factor 2 (RUNX2)	NM_001024630	CGCTGCAACAAGACC	CGCCATGACAGTAACC	900
alkaline phosphatase (ALPL)	NM_000478	ACGTCTTCACATTTGGTG	GGTAGTTGTTGTGAGCATA	450
integrin-binding sialoprotein (IBSP)	NM_004967	GACTGCTTTAATTTTGCTCAG	GTCACTACTGCCCTGAAC	600
secreted phosphoprotein-1 (SPP1)	NM_001040058	CTGACATCCAGTACCCTG	CAGCTGACTCGTTTCATA	600
collagen type 1 alpha 2 chain (COL1A2)	NM_000089	TGAAGCTGGTCCCCAAGGA	AATACCAGGAGCGCGCCGTTG	300

2.11. Statistical Analysis

Statistical analyses were conducted using GraphPad Prism® (version 8.4.0 for Mac OS, La Jolla, CA, USA). Data were expressed as the mean ± standard error of the mean (SE). Group comparisons were executed through one-way ANOVA, followed by Tukey´s multiple comparisons test. Exclusively for the comparison of gene expression, a Mann-Whitney-U test was used. Statistical significance was acknowledged solely when $p \leq 0.05$. Significance levels were denoted by asterisks (*), with *p<0.05, **p<0.01, ***p<0.001 and ****p<0.0001.

 doi:10.20944/preprints202408.0693.v1

3. Results and Discussion

The aim of the study was to explore the combination of alginate, nHA and Col to create a composite ink for 3D bioprinting of constructs capable of replicating the composition of native bone ECM, facilitating *in vitro* studies on osteogenesis and contributing to reducing animal experimentation in the field of tissue engineering.

Alginate was used due to its properties, namely easy adjustability, low price, and accessibility [10,12,37]. Furthermore, the inclusion of nHA, a mineral, and Col, a protein, has been implemented due to their well-known capacity to enhance osteogenic potential and accelerate the regeneration of modular bone tissue [38]. Whilst the inclusion of hydroxyapatite in hydrogels can improve the osteogenic and rheological properties; Col can support high cell viability, proliferation and differentiation, providing an optimal microenvironment conducive to cell survival and functional performance of the printed composite [17,39,40].

The concentrations of alginate, nHA, and Col used in this study (2%, 0.5%, and 0.5%, respectively) were selected based on findings from previous research. According to the literature, 2% alginate provides an optimal environment for cell encapsulation and proliferation [41]. Additionally, the incorporation of 0.5% nHA and 0.5% Col is based on the research conducted by Hassani *et al.*, which demonstrated that these concentrations contribute to an osteogenic microenvironment favourable to the development of bone tissue. These concentration ratios were chosen to leverage their synergistic effects, aiming to enhance the osteogenic differentiation and the overall structural integrity of the hydrogel [25].

The dual crosslinking methodology implemented follows a sequential procedure: Initially, the Col component of the hydrogel undergoes fibrillogenesis induced by raising the temperature to 37°C. Subsequently, the introduction of the $CaCl_2$ solution initiated the ionic crosslinking of alginate. The Col fibrils were subjected to a minimum of 90 minutes of crosslinking to establish stable properties before the addition of $CaCl_2$. Despite the immediate onset of alginate gelation upon contact with Ca^{2+} ions, the crosslinking solution was allowed to interact for 40 minutes. This extended duration ensured comprehensive crosslinking throughout the hydrogel matrix, thereby enhancing its structural and functional integrity [41].

3.1. Rheological Characterization

The viscoelastic characteristics of the crosslinked hydrogels were assessed through oscillatory rheology using amplitude and frequency sweep tests (**Figure 2**). First, the upper limit of the linear viscoelastic region (LVR) was determined from the storage modulus (G') curve assuming a ±5% deviation between two consecutive measurements at 0.1% oscillation strain (Figure 2a).

Amplitude sweep tests (**Figure 2a**) also demonstrated that both formulations exhibited a gel-like or solid structure behaviour in the LVR with a higher G' compared to the G'' (G'>G''). According to literature, viscoelastic solids present a higher storage modulus than loss modulus, due to the strong internal chemical bonds and physicochemical reactions in the material [42]. Considering constant amplitude and frequency conditions (1% strain, 1 Hz frequency), the G' was about ten times higher than the G'', indicating a solid elastic behavior for both formulations. Furthermore, the addition of nHA and Col did not appear to significantly alter LVR ($p>0.05$). Clearly from the results, nHA and Col did not seem to affect the initial characteristics of the hydrogel. The overall modulus of elasticity and loss values did not change between the gels.

Analysing **Figure 2a** also shows that the alginate-nHA-Col group presented a higher yield point (0.00974) compared to the alginate group (0.00864), suggesting that the addition of nHA and Col increased the material's resistance to initial deformation. Meanwhile, the flow point, indicating the transition to a viscous-dominated behavior, was lower in the alginate-nHA-Col group (0.0318) than in the alginate group (0.0685). This data suggest that although the composite hydrogel requires slightly more stress to begin yielding, it transitions to a flow state more readily, possibly due to the combination of the effects of the nHA reinforcement and the elastic behaviour of the Col. To further evaluate the transition from the LVR to the flow state, the flow transition index (ratio of flow point to yield point) was calculated. The alginate group presented a higher index (3.26) compared to the

 doi:10.20944/preprints202408.0693.v1

alginate-nHA-Col group (7.93), suggesting that the alginate-nHA-Col group is less tendency to brittle fracture [43].

Frequency sweeps were conducted within the LVR of both formulations at 0.1% oscillation strain (**Figure 2b**.). The results confirmed viscoelastic gel-like behavior with a clear non-dependence between G′, G″ and frequency. Notably, both formulations showed a consistent 8 kPa difference between G′ and G″ across the tested frequencies. A non-dependence between these values and frequency suggests that the material's elastic and viscous properties were not influenced by the frequency of the applied stress. This is a characteristic of a gel that is stable and does not change its behavior significantly over a range of frequencies. This type of behavior is typical of gels that are well-formed, and it is often noted in materials that are used in applications where they need to maintain their structure and properties over time [44].

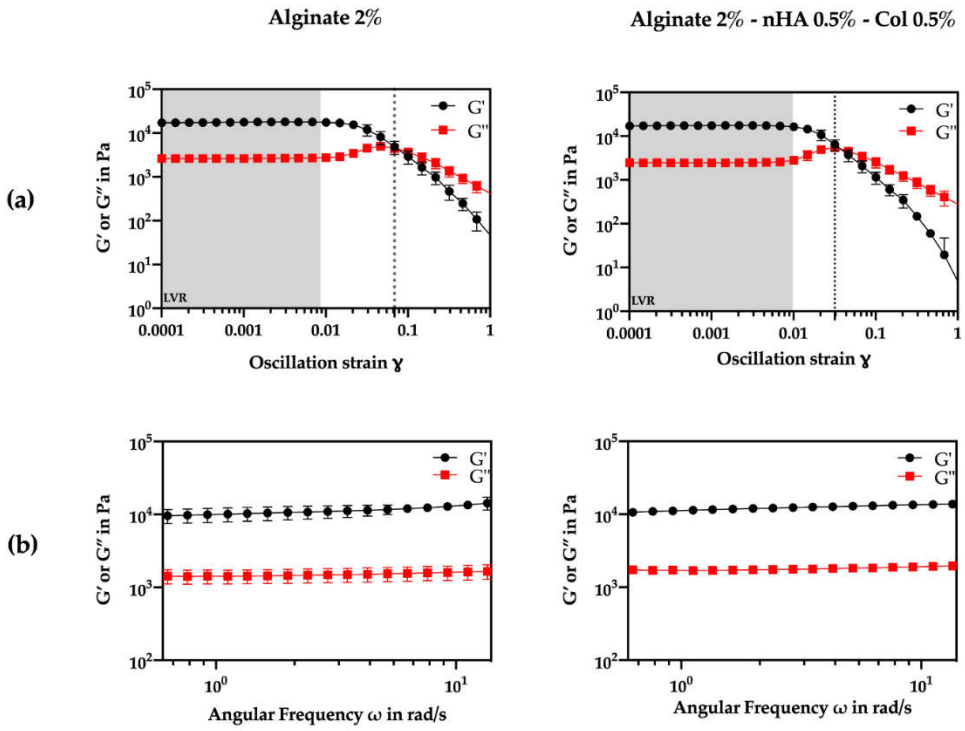

Figure 2. Oscillatory rheological experiments to determine the storage (G′) (black) and loss (G″) (red) moduli of crosslinked alginate 2% and alginate 2% - nHA 0.5% - Col 0.5% over a range of conditions. Measurements were performed in triplicate (n=3). (a) Amplitude sweeps conducted at a frequency of 1 Hz. (b) Frequency sweeps conducted at an oscillation strain of 0.1%.

3.2. Mechanical Analysis

The success of a hydrogel is highly dependent on its mechanical properties, as these properties ensure the hydrogel's structural integrity under both *in vitro* and *in vivo* conditions [45]. Parameters including porosity, pore size, composition, degree of crosslinking, and ionic strength of materials can significantly affect their mechanical strength [46].

The present research assessed the mechanical properties of Alg-based hydrogels using compressive mechanical tests. **Figure 3** and **Table 3** represent the compressive strength-strain curve and Young's modulus of the Alg-based hydrogels, respectively.

Based on the stress-strain curve (**Figure 3**), the alginate-only hydrogel presented a lower stress-strain behavior due to its brittle nature, whereas the composite hydrogel comprising nHA and Col revealed higher stress-strain behavior due to the combined effects of nHA's reinforcement and Col's elasticity. nHA contributed to the reinforcement of the hydrogel matrix, distributing stress more evenly and enhancing the material's toughness and resistance to deformation [46]. On the other hand,

 doi:10.20944/preprints202408.0693.v1

Col, being a fibrous protein, provided elasticity and improved the tensile strength of the hydrogel, providing a more flexible matrix that could stretch further before rupturing [47]. The combination seemed to make the hydrogel more durable and capable of withstanding higher stresses and strains.

Young's modulus was calculated at 10% strain and the addition of 0.5% (w/v) nHA and 0.5% (w/v) of Col 0.5 wt % to alginate decreased Young's modulus of Alg hydrogel from 7.33 to 6.80 MPa (**Table 3**). Notwithstanding, the average Young's modulus of both groups did not show statistically significant differences.

Based on these findings, the hydrogel composed of only alginate appeared to have a higher initial stiffness (higher Young's modulus) but a lower capacity to withstand large deformations (lower stress-strain behaviour) due to its more fragile nature.

Meanwhile, the hydrogel composed of alginate, nHA and Col seemed to be more flexible initially (lower Young's modulus) and better able to withstand large deformations (higher stress-strain behaviour) due to the addition of Col, which increased elasticity, and nHA, which reinforced the matrix.

The combination of the different components in the hydrogel resulted in a material that can better absorb and dissipate stresses, resulting in greater deformation capacity and final strength, despite being initially more flexible.

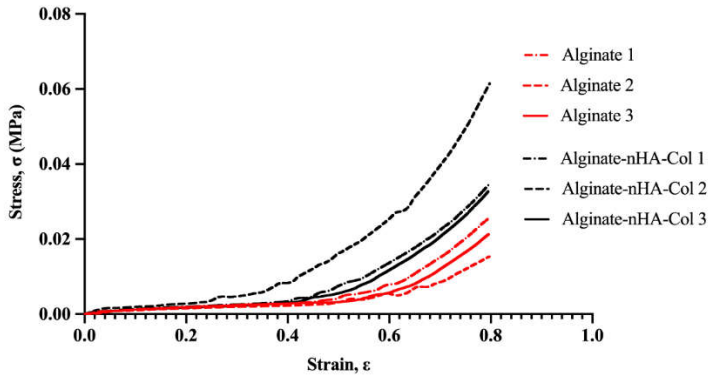

Figure 3. Stress–strain curves obtained from compressive tests of alginate hydrogel (red) and alginate-nHA-Col hydrogel (black) (n=3).

Table 3. Young's modulus measurement of alginate and alginate-nHA-Col hydrogels produced (mean ± sd values) (n=3).

Parameter (MPa)	Alginate	Alginate-nHA-Col (w/v)	P value
Young's Modulus	7.33 ± 1.21	6.80 ± 0.835	0.567

3.3. Hydrogel Swelling Behaviour

The swelling properties play a fundamental role in facilitating the release of molecules, absorption of biofluids, and distribution of nutrients in the structure [38]. Hydrogel swelling behavior (pH = 7.4 at 37°C) was evaluated at time intervals of 1, 2, 3, 4, 5, 24, 48 and 72 hours. The absorption of DPBS by the hydrogels is shown in **Figure 4**. The hydrogels appeared to absorb a significant amount of DPBS at first, and then more gradually over time. The hydrogel appeared to reach swelling equilibrium in a relatively short time (3 hours). The maximum swelling ratio was noted up to 24 hours. Then the swelling ratio significantly dropped in all the hydrogels due to the breakdown of the dry hydrogel system in the presence of DPBS.

Although the data were not significantly different, after 3 hours in culture, the hydrogel with nHA and Col seemed to increase the swelling compared to the hydrogel with alginate only. The incorporation of Col and nHA to alginate can increase the swelling rate of the resulting composite material due to the enhanced stability and mechanical strength of the alginate hydrogel, leading to a

 doi:10.20944/preprints202408.0693.v1

more controlled degradation rate. The incorporation of Col and nHA into alginate matrices may potentially influence the swelling rate of the resulting composite hydrogels. Col, being a hydrophilic material, presents more hydrophilic bonds, which can result in water retention and consequently affect the swelling behavior [48]. Additionally, the hydrophilic nature of hydroxyapatite in the material composition can lead to overall water absorption and potentially enhance cell growth, proliferation, and viability within the material [19]. For bone mimicry, a high degree of swelling is particularly important, as it allows cell infiltration into the hydrogels and maximizes cell growth within the structure [49].

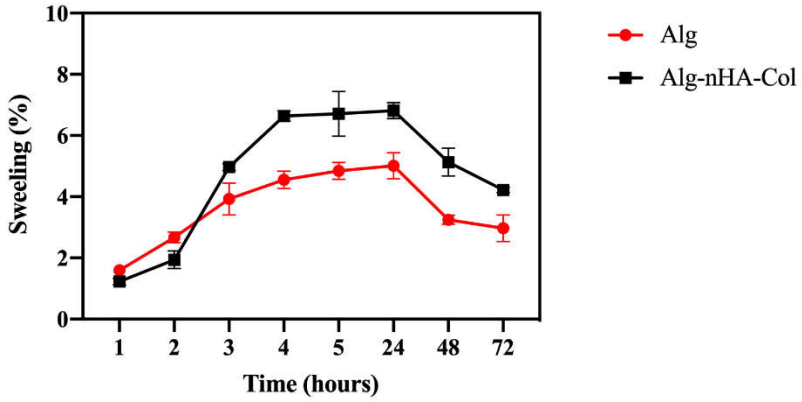

Figure 4. Hydrogel swelling rate from 1 to 72h. Alg: alginate (red); Alg-nHA-Col (black) (n=3).

3.4. Bioprinting of Cell-Laden Hydrogels

This study integrated bioprinting and pressure-assisted extrusion technologies in the printing protocols for alginate-based inks. Firstly, using a RegenHU 3D Discovery Evolution system, the printing was performed with 2% (w/v) alginate biomaterial inks. This formulation was chosen, according to previous works, due to its low viscosity and shear-thinning behavior, resulting in it being appropriate for bioprinting cellular inks [41]. The bioprinting parameters, including needle diameter, pressure, feed speed, filament distance, and thickness, were properly adjusted to establish an optimum equilibrium between printing resolution, speed, and cell activity (**Table 4**). The printing parameters were adjusted to guarantee high cell viability during the printing process whilst ensuring the extrusion of accurate filaments, with the external filament diameter corresponding the internal diameter of the nozzle used. This precision is of paramount importance to ensure the fidelity of the structural form in the final constructs, thus achieving an accurate physical replication of the digital CAD model (**Figure 5-A, B and C**).

Due to the low viscosity of the bioink formulations used, without compromising shape fidelity [41], suspension bioprinting strategies were adopted: a support agarose bath (0.5% (w/v)) that maintains the structure of the printed material in suspension (**Figure 5-D**). Once the material had been deposited and crosslinked, the suspension bath was removed and the hydrogels with the cells could grow.

Table 4. Parameters used in the RegenHU 3D Discovery Evolution system. The values are shown in the respective units.

Parameters	Values (unit)
Needle Diameter	600 µm
Pressure	0.02 MPa
Feed Rate	10 mm/s
Filament Distance	500 mm
Thickness	500 mm

 doi:10.20944/preprints202408.0693.v1

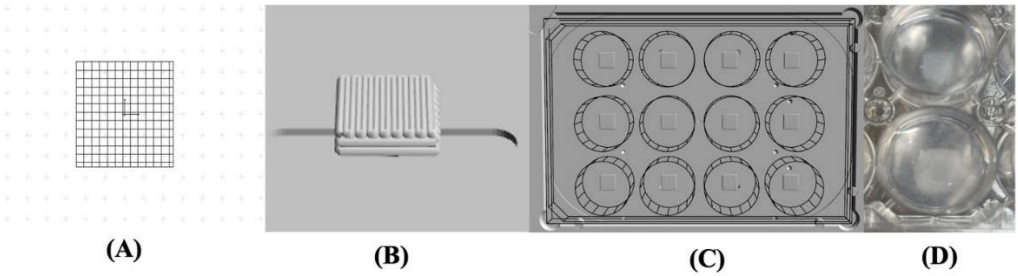

Figure 5. (A) CAD model designed in BioCAD™ software; (B) 3D generated model; (C) 3D generated model in a 12-well plate; (D) Cell-laden print in the agarose support bath.

3.5. Live/Dead Staining

Cell viability must be maintained both during and after the 3D tissue printing process. Therefore, a assessment of cell viability (hBMSCs) was performed using a Live/Dead analysis. This analysis was conducted after 1, 3, and 7 days in culture (**Figure 6-A and B**).

The staining demonstrated high levels of cell viability in both alginate and alginate-nHA-Col hydrogels throughout all time points (**Figure 6-A).**

The hBMSCs viability and distribution did not appear to depend on the inclusion of nHA and Col to the gel and the cells seemed to be homogeneously distributed in both hydrogels. In fact, some cell death was observed throughout the experiment, although this was to be expected due to exposure to significant shear stress during the printing process, which can cause cell damage and death [50]. Nevertheless, the results of the alginate-nHA-Col group indicated that live cell portions remained above 80% one week after processing (**Figure 6-B).** It is important to note that alginate-nHA-Col group presented slightly higher values of cell viability, but with no significant differences when compared to the alginate group throughout the experiment.

In addition, data showed that a spherical cell morphology was preserved throughout the culture in both conditions. The spherical shape of cells within a bioink is preferable to ensure the cell viability and functionality throughout the bioprinting process to maintain their native structure and function, which is crucial for their differentiation into specific cell lineages for tissue engineering applications [51].

These findings suggest that alginate-nHA-Col hydrogels were not cytotoxic and provided a supportive matrix that promotes high cell viability of hBMSCs cultured. The outcomes confirmed that the formulated hydrogels can maintain hBMSCs in culture and propose that pressure-assisted extrusion did not have a prejudicial effect on cell viability.

 doi:10.20944/preprints202408.0693.v1

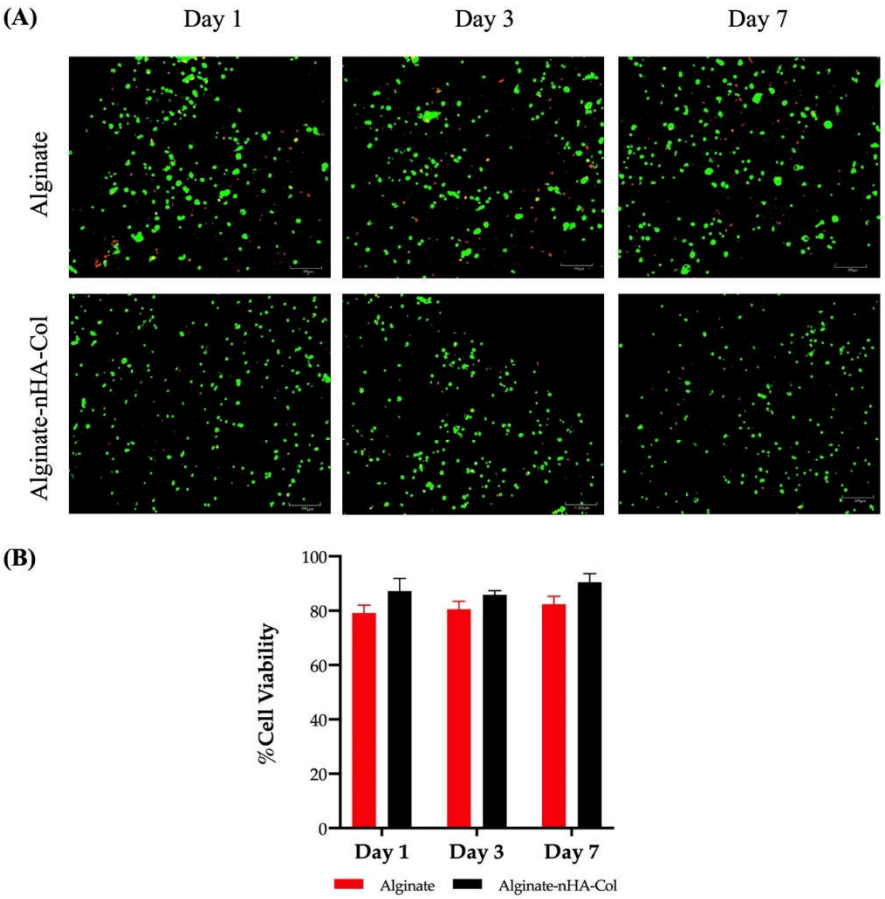

Figure 6. (A) Live/Dead staining of bioprinted hBMSCs cultured in 2% alginate and 2% alginate - 0.5% nHA - 0.5% Col for 1, 3 and 7 days. Live cells were stained green by calcein, and dead cells were stained red by EthD-1. (B) The percentage of cell viability of bioprinted hBMSCs cultured in 2% alginate and 2% alginate - 0.5% nHA - 0.5% Col for 1, 3 and 7 days (n=3).

3.6. Cell Viability Assay

In accordance with the ISO 10993-5:2009 guidelines, the assessment of cellular viability was determined using PrestoBlue™ on both alginate and alginate-nHA-Col hydrogels in the presence of hBMSCs. The control group, devoid of hydrogels was also included for reference. **Figure 7-A** represents the corrected absorbance values for the designated time points (1, 3, 5, and 7 days). The data showed cell proliferation in all groups up to day 5. Although the hydrogels with alginate, nHA and Col presented slightly higher cell viability rates when compared with the other groups, only at day 3 were statistically significant differences identified. Conversely, alginate-nHA-Col demonstrated significantly higher absorbance than the control group, suggesting evidence of induction of cell adhesion and proliferation. Current data is in accordance with previous study, indicating that alginate-nHA-Col hydrogels presented, overall, a superior cytocompatibility performance when in comparison with the control group [25].

The results of the percentage of viability inhibition normalized to the control group are presented in **Figure 7-B**. In accordance with Annex 3 of the ISO 10993-5:2009 guideline, a cytotoxic effect is considered when an inhibition of viability larger than 30% is identified (outlined in **Figure 7-B** by dashed lines). These findings suggest that both alginate and alginate-nHA-Col can be classified as non-cytotoxic.

In agreement with the results presented in the Live/Dead analysis, the viability results confirmed that, on one hand, the hydrogels are supportive of hBMSCs encapsulation and function and, on the

 doi:10.20944/preprints202408.0693.v1

other, the printing process does not negatively impact on cell survival that remained viable for up to seven days post-encapsulation.

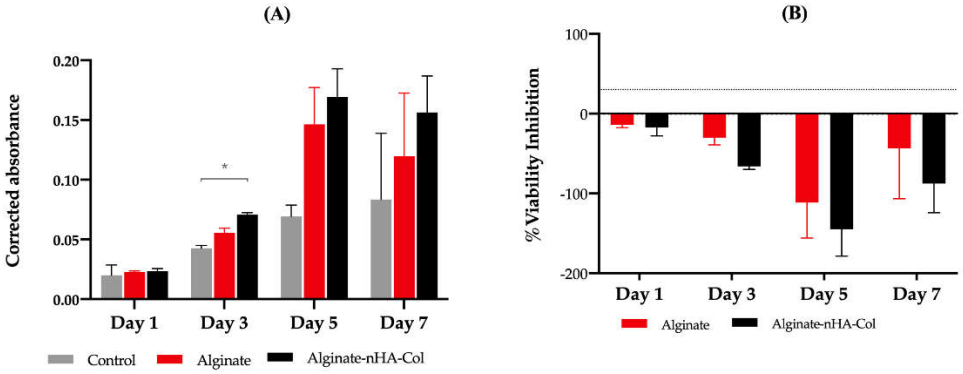

Figure 7. (A) Corrected absorbance evaluated by Presto Blue® viability assay for hBMSCs. Results significance are presented through the symbol (*), according to the P value, with *p<0.05. The absorbance was corrected by subtracting the average of the blank wells (average of 570-595 nm) from the absorbance values (570-595 nm) of each experimental group. (B) % viability inhibition evaluated by PrestoBlue® viability assay for hBMSCs. Results were normalised to the control as 0%. The 30% threshold presented in the graph (dashed line) indicates the inhibition above which the effect is classified as cytotoxic (under ISO 10993-5:2009 guidelines).

3.7. Gene Expression

Osteogenesis of hBMSCs cultured in alginate and alginate-nHA-Col for 7 and 14 days was evaluated using qPCR for a panel of key differentiation marker genes (**Figure 8**). This gene expression analysis provided insights into the biofunctionality and osteoinductive potential of the bioinks for bone tissue engineering applications.

After 14 days of culture, gene expression analysis revealed a higher expression of osteogenic markers (**Figure 8**) in all experimental groups compared to the same groups after 7 days. The relative expression levels of RUNX2 in the alginate-nHA-Col group were slightly higher than the alginate group at both timepoints (**Figure 8-A**). RUNX2 plays a crucial role in regulating the osteogenic differentiation of hBMSCs and presence of this gene leads to the formation of mature osteoblasts and complete bone formation [52]. ALPL is associated with the biological process of endochondral ossification/ osteoblast differentiation [53] and showed a minimal increase from day 7 to day 14 (Figure 8-B). Gene expression of IBSP demonstrated an increase in both groups from 7 to 14 days (Figure 8-C). IBSP expression has been shown to increase the expression of key osteogenic and angiogenic markers, indicating its beneficial role in promoting the formation and vascularisation of bone tissue [54,55].

Although not statistically significant, the expression of SPP1 in the alginate group was higher than in the alginate-nHA-Col group (**Figure 8-D**). SPP1 is a crucial component of the organic matrix of bone and serves as a binding protein for osteoclasts, the cells responsible for bone remodeling [56].

COL1A2 was not expressed in any of the groups after 7 days (**Figure 8-E**). However, after 14 days, the alginate-nHA-Col group showed an up-regulation of COL1A2 expression compared to the alginate group. Col is a major ECM protein synthesized by osteoblasts and significantly contributes to bone strength [57]. The observed increased expression of these osteoblastic genes in 3D hBMSCs constructs after 14 days suggests that the incorporation of alginate, nHA and Col elements in the bioink is important for enhancing osteogenic differentiation.

The presence of bone-related gene expression in alginate-nHa-Col at day 14 also suggests a positive and sustained long-term osteogenic effect in hBMSCs. Nevertheless, osteogenic differentiation is a complex process that involves the sequential expression of several genetic markers at different times. For instance, early markers such as RUNX2 and osterix are expressed during the

 doi:10.20944/preprints202408.0693.v1

initial phases of differentiation, while later markers such as SPP1 and osteocalcin are associated with mature osteoblasts and mineralization [58]. As future research, it is important to evaluate genetic markers over an extended period, such as 21 days. In addition, further studies, such as staining with ALP and Alizarin Red, would be pertinent in providing better validation of the support's functionality and osteogenic differentiation.

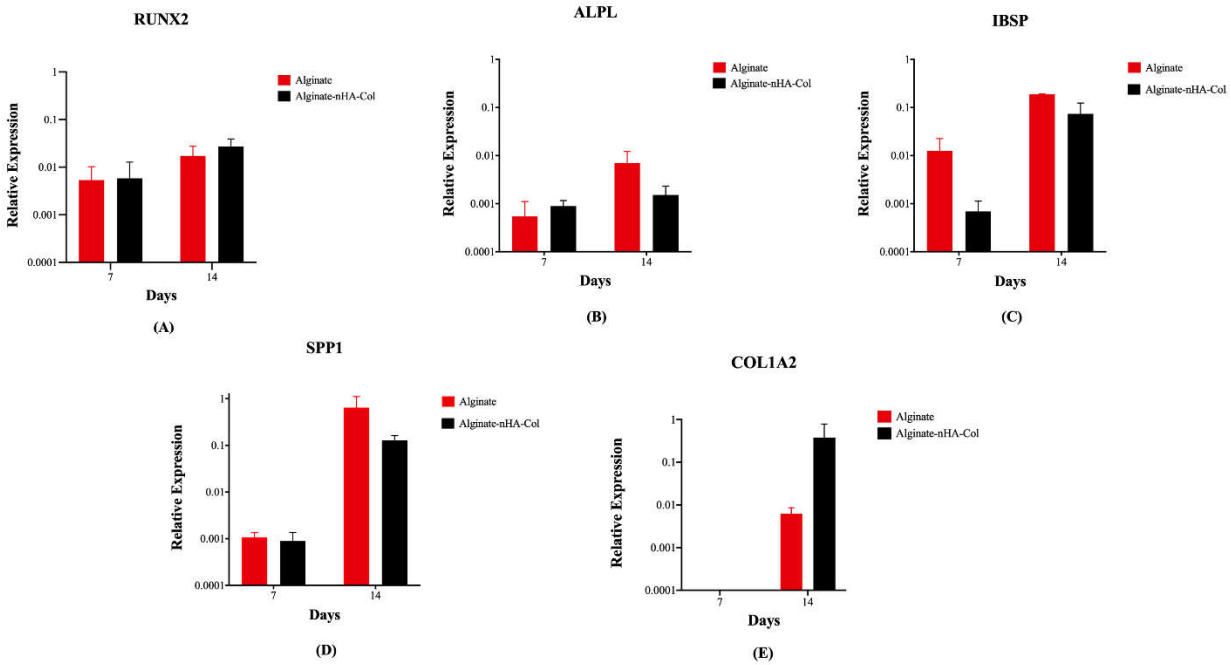

Figure 8. Gene expression levels of printed hBMSCs in alginate and alginate-nHA-Col bioinks following 7 and 14 days under osteogenic differentiation: runt-related transcription factor 2 (RUNX2) (A), alkaline phosphatase (ALPL) (B), integrin-binding sialoprotein (IBSP) (C), secreted phosphoprotein-1 (SPP1) (D) and collagen type 1 alpha 2 chain (COL1A2) (E).

4. Conclusions

The present study describes the successful development of a composite hydrogel bioink based on incorporated alginate, nHA, and Col, along with hBMSCs.

Rheological tests confirm that the viscoelastic properties are maintained with the addition of nHA and Col, while the mechanical tests showed that these additions enhance the hydrogel's performance under compressive stresses. LIVE/DEAD™ and PrestoBlue results confirm the ability of developed materials to support the encapsulation and printing of hBMSCs without significant loss cell viability 7 days post-printing. PCR analysis demonstrated that the alginate-nHA-col enhanced the expression of osteogenic markers in hBMSCs, suggesting the hydrogel's pro-osteogenic differentiation potential.

The incorporation of nHA and Col into alginate appears to have enhanced the physical and biological properties of the bioink, providing a promising 3D bioprinted model to mimic bone tissue. This study represents a significant step forward in the development of bioinks for this field, offering a viable and ethical solution for studying osteogenesis and early tissue maturation *in vitro*.

This approach intends to pave the way for advances in bone tissue engineering, contributing to improved therapeutic strategies for bone-related diseases.

Author Contributions: For research articles with several authors, a short paragraph specifying their individual contributions must be provided. The following statements should be used "Conceptualization, A.C.S., M.D. and A.C.M.; methodology, A.C.S., G.M. and F.S.; validation, A.C.S., G.M. and F.S.; formal analysis, A.C.S., G.M., F.S. and M.D.; investigation, A.C.S., G.M., F.S., R.A., B.L., P.S., A.M. and A.C.; resources, J.D.S., L.A., N.A., S.R., M.D. and A.C.M..; data curation, A.C.S., G.M. and F.S.; writing—original draft preparation, A.C.S.; writing—review and editing, A.C.S., G.M., F.S., R.A., B.L., P.S., A.M., A.C., J.D.S., L.A., N.A., S.R., M.D. and A.C.M.; visualization,

 doi:10.20944/preprints202408.0693.v1

A.C.S., G.M., F.S., R.A., B.L., P.S., A.M., A.C., J.D.S., L.A., N.A., S.R., M.D. and A.C.M.; supervision, J.D.S., L.A., N.A., S.R., M.D. and A.C.M.; project administration, M.D. and A.C.M; funding acquisition, S.R., M.D. and A.C.M. All authors have read and agreed to the published version of the manuscript.

Funding: Ana Catarina Sousa (SFRH/BD/146689/2019), Bruna Lopes (2021.05265.BD), Patrícia Sousa (2023.00246.BD), André Coelho (2023.00428.BD), Alícia Moreira (2023.00544.BD) and acknowledge Fundação para a Ciência e Tecnologia (FCT), for financial support. Rui Alvites acknowledges the CECA, UP, and FCT for the funding and accessibility of all technical, structural, and human resources necessary for the development of this work. The work was supported through the project UIDB/00211/2020 funded by FCT/MCTES, national funds. This research was funded by Projects PEst-OE/AGR/UI0211/2011 from FCT, and COM-PETE 2020, from ANI–Projetos ID&T Empresas em Copromoção, by the project "InnovaBIOMAS - Optimized Additive Biofabrication System for the Production of Hierarchical Multi-Tissue Scaffolds Applied in the Treatment of Joint Diseases" with the reference 2022.10564.PTDC, by the project "Bone2Move- Development of "in vivo" experimental techniques and modelling methodologies for the evaluation of 4D scaffolds for bone defect in sheep model: an integrative research approach" with the reference POCI-01-0145-FEDER-031146. Marco Domingos would like to thank the Henry Royce Institute EPSRC grants EP/R00661X/1, EP/S019367/1, EP/P025021/1 and EP/P025498/1.

Institutional Review Board Statement: The study was conducted in accordance with the Declaration of Helsinki and approved by the NHS Health Research Authority National Research Ethics Service (number: 21/NS/0056) and the University of Manchester.

Informed Consent Statement: All experiments followed the relevant guidelines and were conducted with approvals from the NHS Health Research Authority National Research Ethics Service (number: 21/NS/0056) and the University of Manchester, as well as written inform donor consent.

Data Availability Statement: Not applicable.

Acknowledgments: Not applicable.

Conflicts of Interest: The authors declare no conflicts of interest.

List of Abbreviations:

3D	three-dimensional
ALPL	alkaline phosphatase
$CaCl_2$	calcium chloride
Col	collagen
COL1A2	collagen type 1 alpha 2 chain
DPBS	dulbecco's phosphate-buffered saline
ECM	extracellular matrix
FBS	fetal bovine serum
G'	storage modulus
G''	loss modulus
IBSP	integrin-binding sialoprotein
hBMSC	human bone marrow stem/stromal cell
HA	hydroxyapatite
LVR	linear viscoelastic region
MSC	mesenchymal stem/stromal cell
nHA	nano-hydroxyapatite
qPCR	quantitative real-time polymerase chain reaction
RUNX2	runt-related transcription factor 2
SPP1	secreted phosphoprotein-1
SE	standard deviation of the mean

References

1. Wu, A.-M.; Bisignano, C.; James, S.L.; Abady, G.G.; Abedi, A.; Abu-Gharbieh, E.; Alhassan, R.K.; Alipour, V.; Arabloo, J.; Asaad, M.; et al. Global, regional, and national burden of bone fractures in 204 countries and territories, 1990–2019: a systematic analysis from the Global Burden of Disease Study 2019. *The Lancet Healthy Longevity* **2021**, *2*, e580-e592, doi:10.1016/S2666-7568(21)00172-0.
2. Polinder, S.; Haagsma, J.; Panneman, M.; Scholten, A.; Brugmans, M.; Van Beeck, E. The economic burden of injury: Health care and productivity costs of injuries in the Netherlands. *Accid Anal Prev* **2016**, *93*, 92-100, doi:10.1016/j.aap.2016.04.003.

3. Borgström, F.; Karlsson, L.; Ortsäter, G.; Norton, N.; Halbout, P.; Cooper, C.; Lorentzon, M.; McCloskey, E.V.; Harvey, N.C.; Javaid, M.K.; et al. Fragility fractures in Europe: burden, management and opportunities. *Arch Osteoporos* **2020**, *15*, 59, doi:10.1007/s11657-020-0706-y.
4. Caddeo, S.; Boffito, M.; Sartori, S. Tissue Engineering Approaches in the Design of Healthy and Pathological In Vitro Tissue Models. *Front Bioeng Biotechnol* **2017**, *5*, 40, doi:10.3389/fbioe.2017.00040.
5. Owen, R.; Reilly, G.C. In vitro Models of Bone Remodelling and Associated Disorders. *Frontiers in Bioengineering and Biotechnology* **2018**, *6*, doi:10.3389/fbioe.2018.00134.
6. Tripathi, S.; Mandal, S.S.; Bauri, S.; Maiti, P. 3D bioprinting and its innovative approach for biomedical applications. *MedComm (2020)* **2023**, *4*, e194, doi:10.1002/mco2.194.
7. Im, S.; Choe, G.; Seok, J.M.; Yeo, S.J.; Lee, J.H.; Kim, W.D.; Lee, J.Y.; Park, S.A. An osteogenic bioink composed of alginate, cellulose nanofibrils, and polydopamine nanoparticles for 3D bioprinting and bone tissue engineering. *International Journal of Biological Macromolecules* **2022**, *205*, 520-529, doi:https://doi.org/10.1016/j.ijbiomac.2022.02.012.
8. Gonzalez-Fernandez, T.; Sikorski, P.; Leach, J.K. Bio-instructive materials for musculoskeletal regeneration. *Acta Biomater* **2019**, *96*, 20-34, doi:10.1016/j.actbio.2019.07.014.
9. Gonzalez-Fernandez, T.; Tenorio, A.J.; Campbell, K.T.; Silva, E.A.; Leach, J.K. Alginate-Based Bioinks for 3D Bioprinting and Fabrication of Anatomically Accurate Bone Grafts. *Tissue Eng Part A* **2021**, *27*, 1168-1181, doi:10.1089/ten.TEA.2020.0305.
10. Datta, S. Advantage of Alginate Bioinks in Biofabrication for Various Tissue Engineering Applications. *International Journal of Polymer Science* **2023**, *2023*, 6661452, doi:https://doi.org/10.1155/2023/6661452.
11. Mahmud, R.U.; Rahman, M.Z. 13.13 - Synthesis and characterization of nanocomposites for tissue engineering. In *Comprehensive Materials Processing (Second Edition)*, Hashmi, S., Ed.; Elsevier: Oxford, 2024; pp. 241-269.
12. Hariyadi, D.M.; Islam, N. Current Status of Alginate in Drug Delivery. *Advances in Pharmacological and Pharmaceutical Sciences* **2020**, *2020*, 8886095, doi:https://doi.org/10.1155/2020/8886095.
13. Shams, E.; Barzad, M.S.; Mohamadnia, S.; Tavakoli, O.; Mehrdadfar, A. A review on alginate-based bioinks, combination with other natural biomaterials and characteristics. *Journal of Biomaterials Applications* **2022**, *37*, 355-372, doi:10.1177/08853282221085690.
14. Sudipto, D.; Ranjit, B.; Jonali, D. Importance of Alginate Bioink for 3D Bioprinting in Tissue Engineering and Regenerative Medicine. In *Alginates*, Leonel, P., Ed.; IntechOpen: Rijeka, 2019; p. Ch. 7.
15. Ma, C.; Du, T.; Niu, X.; Fan, Y. Biomechanics and mechanobiology of the bone matrix. *Bone Research* **2022**, *10*, 59, doi:10.1038/s41413-022-00223-y.
16. Bielajew, B.J.; Hu, J.C.; Athanasiou, K.A. Collagen: quantification, biomechanics and role of minor subtypes in cartilage. *Nature Reviews Materials* **2020**, *5*, 730-747, doi:10.1038/s41578-020-0213-1.
17. Li, Z.; Ruan, C.; Niu, X. Collagen-based bioinks for regenerative medicine: Fabrication, application and prospective. *Medicine in Novel Technology and Devices* **2023**, *17*, 100211, doi:https://doi.org/10.1016/j.medntd.2023.100211.
18. Li, Y.; Liu, Y.; Li, R.; Bai, H.; Zhu, Z.; Zhu, L.; Zhu, C.; Che, Z.; Liu, H.; Wang, J.; et al. Collagen-based biomaterials for bone tissue engineering. *Materials & Design* **2021**, *210*, 110049, doi:https://doi.org/10.1016/j.matdes.2021.110049.
19. Sousa, A.C.; Biscaia, S.; Alvites, R.; Branquinho, M.; Lopes, B.; Sousa, P.; Valente, J.; Franco, M.; Santos, J.D.; Mendonça, C.; et al. Assessment of 3D-Printed Polycaprolactone, Hydroxyapatite Nanoparticles and Diacrylate Poly(ethylene glycol) Scaffolds for Bone Regeneration. *Pharmaceutics* **2022**, *14*, doi:10.3390/pharmaceutics14122643.
20. Sancilio, S.; Gallorini, M.; Di Nisio, C.; Marsich, E.; Di Pietro, R.; Schweikl, H.; Cataldi, A. Alginate/Hydroxyapatite-Based Nanocomposite Scaffolds for Bone Tissue Engineering Improve Dental Pulp Biomineralization and Differentiation. *Stem Cells Int* **2018**, *2018*, 9643721, doi:10.1155/2018/9643721.
21. Quinlan, E.; López-Noriega, A.; Thompson, E.; Kelly, H.M.; Cryan, S.A.; O'Brien, F.J. Development of collagen-hydroxyapatite scaffolds incorporating PLGA and alginate microparticles for the controlled delivery of rhBMP-2 for bone tissue engineering. *J Control Release* **2015**, *198*, 71-79, doi:10.1016/j.jconrel.2014.11.021.
22. Soleymani, S.; Naghib, S.M. 3D and 4D printing hydroxyapatite-based scaffolds for bone tissue engineering and regeneration. *Heliyon* **2023**, *9*, e19363, doi:https://doi.org/10.1016/j.heliyon.2023.e19363.
23. Melo, P.; Montalbano, G.; Fiorilli, S.; Vitale-Brovarone, C. 3D Printing in Alginic Acid Bath of In-Situ Crosslinked Collagen Composite Scaffolds. *Materials (Basel)* **2021**, *14*, doi:10.3390/ma14216720.
24. Chen, Y.; Zhou, Y.; Wang, C. Investigation of Collagen-Incorporated Sodium Alginate Bioprinting Hydrogel for Tissue Engineering. *Journal of Composites Science* **2022**, *6*, 227.
25. Hassani, A.; Khoshfetrat, A.B.; Rahbarghazi, R.; Sakai, S. Collagen and nano-hydroxyapatite interactions in alginate-based microcapsule provide an appropriate osteogenic microenvironment for modular bone tissue formation. *Carbohydrate Polymers* **2022**, *277*, 118807, doi:https://doi.org/10.1016/j.carbpol.2021.118807.

26. Campos, J.M.; Sousa, A.C.; Caseiro, A.R.; Pedrosa, S.S.; Pinto, P.O.; Branquinho, M.V.; Amorim, I.; Santos, J.D.; Pereira, T.; Mendonça, C.M.; et al. Dental pulp stem cells and Bonelike(®) for bone regeneration in ovine model. *Regen Biomater* **2019**, *6*, 49-59, doi:10.1093/rb/rby025.
27. Merimi, M.; El Majzoub, R.; Lagneaux, L.; Agha, D.; Fatima, B.; Meuleman, N.; Fahmi, H.; Lewalle, P.; Mohammad, F.-K.; Najar, M. The Therapeutic Potential of Mesenchymal Stromal Cells for Regenerative Medicine: Current Knowledge and Future Understandings. *Frontiers in Cell and Developmental Biology* **2021**, *9*, doi:10.3389/fcell.2021.661532.
28. Aleynik, D.; Charykova, I.; Rubtsova, Y.; Linkova, D.; Farafontova, E.; Egorikhina, M. Specific Features of the Functional Activity of Human Adipose Stromal Cells in the Structure of a Partial Skin-Equivalent. *International Journal of Molecular Sciences* **2024**, *25*, 6290, doi:10.3390/ijms25126290.
29. Sai, B.; Dai, Y.; Fan, S.; Wang, F.; Wang, L.; Li, Z.; Tang, J.; Wang, L.; Zhang, X.; Zheng, L.; et al. Cancer-educated mesenchymal stem cells promote the survival of cancer cells at primary and distant metastatic sites via the expansion of bone marrow-derived-PMN-MDSCs. *Cell Death & Disease* **2019**, *10*, 941, doi:10.1038/s41419-019-2149-1.
30. Kemp, K.C.; Hows, J.; Donaldson, C. Bone marrow-derived mesenchymal stem cells. *Leuk Lymphoma* **2005**, *46*, 1531-1544, doi:10.1080/10428190500215076.
31. Strassburg, S.; Richardson, S.M.; Freemont, A.J.; Hoyland, J.A. Co-culture induces mesenchymal stem cell differentiation and modulation of the degenerate human nucleus pulposus cell phenotype. *Regen Med* **2010**, *5*, 701-711, doi:10.2217/rme.10.59.
32. Senior, J.J.; Cooke, M.E.; Grover, L.M.; Smith, A.M. Fabrication of Complex Hydrogel Structures Using Suspended Layer Additive Manufacturing (SLAM). *Advanced Functional Materials* **2019**, *29*, 1904845, doi:https://doi.org/10.1002/adfm.201904845.
33. Moxon, S.R.; Cooke, M.E.; Cox, S.C.; Snow, M.; Jeys, L.; Jones, S.W.; Smith, A.M.; Grover, L.M. Suspended Manufacture of Biological Structures. *Advanced Materials* **2017**, *29*, 1605594, doi:https://doi.org/10.1002/adma.201605594.
34. Minogue, B.M.; Richardson, S.M.; Zeef, L.A.; Freemont, A.J.; Hoyland, J.A. Characterization of the human nucleus pulposus cell phenotype and evaluation of novel marker gene expression to define adult stem cell differentiation. *Arthritis Rheum* **2010**, *62*, 3695-3705, doi:10.1002/art.27710.
35. Minogue, B.M.; Richardson, S.M.; Zeef, L.A.; Freemont, A.J.; Hoyland, J.A. Transcriptional profiling of bovine intervertebral disc cells: implications for identification of normal and degenerate human intervertebral disc cell phenotypes. *Arthritis Res Ther* **2010**, *12*, R22, doi:10.1186/ar2929.
36. Livak, K.J.; Schmittgen, T.D. Analysis of Relative Gene Expression Data Using Real-Time Quantitative PCR and the 2−ΔΔCT Method. *Methods* **2001**, *25*, 402-408, doi:https://doi.org/10.1006/meth.2001.1262.
37. Datta, S. Advantage of alginate bioinks in biofabrication for various tissue engineering applications. *International Journal of Polymer Science* **2023**, *2023*.
38. Hassani, A.; Avci, Ç.B.; Kerdar, S.N.; Amini, H.; Amini, M.; Ahmadi, M.; Sakai, S.; Bagca, B.G.; Ozates, N.P.; Rahbarghazi, R.; et al. Interaction of alginate with nano-hydroxyapatite-collagen using strontium provides suitable osteogenic platform. *Journal of Nanobiotechnology* **2022**, *20*, 310, doi:10.1186/s12951-022-01511-9.
39. Ojeda, E.; García-Barrientos, Á.; Martínez de Cestafe, N.; Alonso, J.M.; Pérez-González, R.; Sáez-Martínez, V. Nanometric Hydroxyapatite Particles as Active Ingredient for Bioinks: A Review. *Macromol* **2022**, *2*, 20-29, doi:10.3390/macromol2010002.
40. Li, N.; Guo, R.; Zhang, Z.J. Bioink Formulations for Bone Tissue Regeneration. *Front Bioeng Biotechnol* **2021**, *9*, 630488, doi:10.3389/fbioe.2021.630488.
41. Ferreira, M.J.S.L.M. Integrating 3D Bioprinting and Pluripotent Stem Cell Technologies for Articular Cartilage Tissue Engineering. The University of Manchester, 2022.
42. Kostenko, A.; Connon, C.J.; Swioklo, S. Storable Cell-Laden Alginate Based Bioinks for 3D Biofabrication. *Bioengineering (Basel)* **2022**, *10*, doi:10.3390/bioengineering10010023.
43. Paar, A. Amplitude sweeps. Available online: https://wiki.anton-paar.com/uk-en/amplitude-sweeps/#:~:text=The%20limit%20of%20the%20linear,with%20the%20lowest%20strain%20values. (accessed on 31-12-2024).
44. Kocen, R.; Gasik, M.; Gantar, A.; Novak, S. Viscoelastic behaviour of hydrogel-based composites for tissue engineering under mechanical load. *Biomedical Materials* **2017**, *12*, 025004, doi:10.1088/1748-605X/aa5b00.
45. Shaabani, A.; Sedghi, R.; Motasadizadeh, H.; Dinarvand, R. Self-healable conductive polyurethane with the body temperature-responsive shape memory for bone tissue engineering. *Chemical Engineering Journal* **2021**, *411*, 128449, doi:https://doi.org/10.1016/j.cej.2021.128449.
46. Martinez, A.W.; Caves, J.M.; Ravi, S.; Li, W.; Chaikof, E.L. Effects of crosslinking on the mechanical properties, drug release and cytocompatibility of protein polymers. *Acta Biomaterialia* **2014**, *10*, 26-33, doi:https://doi.org/10.1016/j.actbio.2013.08.029.
47. Yi, B.; Xu, Q.; Liu, W. An overview of substrate stiffness guided cellular response and its applications in tissue regeneration. *Bioact Mater* **2022**, *15*, 82-102, doi:10.1016/j.bioactmat.2021.12.005.

48. Naomi, R.; Ridzuan, P.M.; Bahari, H. Current Insights into Collagen Type I. *Polymers (Basel)* **2021**, *13*, doi:10.3390/polym13162642.
49. Iviglia, G.; Cassinelli, C.; Torre, E.; Baino, F.; Morra, M.; Vitale-Brovarone, C. Novel bioceramic-reinforced hydrogel for alveolar bone regeneration. *Acta Biomaterialia* **2016**, *44*, 97-109, doi:https://doi.org/10.1016/j.actbio.2016.08.012.
50. Fischer, L.; Nosratlo, M.; Hast, K.; Karakaya, E.; Ströhlein, N.; Esser, T.U.; Gerum, R.; Richter, S.; Engel, F.B.; Detsch, R.; et al. Calcium supplementation of bioinks reduces shear stress-induced cell damage during bioprinting. *Biofabrication* **2022**, *14*, 045005, doi:10.1088/1758-5090/ac84af.
51. Wu, Z.; Su, X.; Xu, Y.; Kong, B.; Sun, W.; Mi, S. Bioprinting three-dimensional cell-laden tissue constructs with controllable degradation. *Scientific Reports* **2016**, *6*, 24474, doi:10.1038/srep24474.
52. Du, L.; Qin, C.; Zhang, H.; Han, F.; Xue, J.; Wang, Y.; Wu, J.; Xiao, Y.; Huan, Z.; Wu, C. Multicellular Bioprinting of Biomimetic Inks for Tendon-to-Bone Regeneration. *Advanced Science* **2023**, *10*, 2301309, doi:https://doi.org/10.1002/advs.202301309.
53. Fideles, S.O.M.; Ortiz, A.C.; Assis, A.F.; Duarte, M.J.; Oliveira, F.S.; Passos, G.A.; Beloti, M.M.; Rosa, A.L. Effect of cell source and osteoblast differentiation on gene expression profiles of mesenchymal stem cells derived from bone marrow or adipose tissue. *J Cell Biochem* **2019**, *120*, 11842-11852, doi:10.1002/jcb.28463.
54. Kriegel, A.; Schlosser, C.; Habeck, T.; Dahmen, C.; Götz, H.; Clauder, F.; Armbruster, F.P.; Baranowski, A.; Drees, P.; Rommens, P.M.; et al. Bone Sialoprotein Immobilized in Collagen Type I Enhances Bone Regeneration In vitro and In vivo. *Int J Bioprint* **2022**, *8*, 591, doi:10.18063/ijb.v8i3.591.
55. Kriegel, A.; Langendorf, E.; Kottmann, V.; Kämmerer, P.W.; Armbruster, F.P.; Wiesmann-Imilowski, N.; Baranowski, A.; Gercek, E.; Drees, P.; Rommens, P.M.; et al. Bone Sialoprotein Immobilized in Collagen Type I Enhances Angiogenesis In Vitro and In Ovo. *Polymers* **2023**, *15*, 1007.
56. Singh, A.; Gill, G.; Kaur, H.; Amhmed, M.; Jakhu, H. Role of osteopontin in bone remodeling and orthodontic tooth movement: a review. *Progress in Orthodontics* **2018**, *19*, doi:10.1186/s40510-018-0216-2.
57. Viguet-Carrin, S.; Garnero, P.; Delmas, P.D. The role of collagen in bone strength. *Osteoporos Int* **2006**, *17*, 319-336, doi:10.1007/s00198-005-2035-9.
58. Gromolak, S.; Krawczenko, A.; Antończyk, A.; Buczak, K.; Kiełbowicz, Z.; Klimczak, A. Biological Characteristics and Osteogenic Differentiation of Ovine Bone Marrow Derived Mesenchymal Stem Cells Stimulated with FGF-2 and BMP-2. *Int J Mol Sci* **2020**, *21*, doi:10.3390/ijms21249726.